INT. J. HYPERTHERMIA, 1992, VOL. 8, NO. 6, 831–842

Insonation of fixed porcine kidney by a prototype sector-vortex-phased array applicator

S.-I. UMEMURA*†, K. R. HOLMES‡, L. A. FRIZZELL§ and C. A. CAIN¶

†Advanced Research Laboratory, Hitachi Ltd, Hatoyama, Saitama 350–03, Japan
‡Department of Veterinary Bioscience and Bioengineering Faculty, and §Bioacoustics Research Laboratory, Department of Electrical and Computer Engineering, University of Illinois, Urbana, IL 61801, USA
¶Bioengineering Program, University of Michigan, Ann Arbor, MI 48109, USA

(*Received 30 October 1991; revised 12 May 1992; accepted 14 May 1992*)

The sector-vortex applicator, an ultrasound phased array with a geometric focus having multiple sectors and tracks, can directly synthesize, without scanning, diffuse focal patterns useful for hyperthermia. A perfused tissue phantom, consisting of an alcohol-fixed porcine kidney with thermocouples placed in the cortex, is insonated by a prototype sector-vortex applicator with 16 sectors and two tracks at an ultrasound frequency of 750 kHz. Steady-state temperature distributions are measured for a wide range of perfusion rates. Results demonstrate that the radius of the heated region can be controlled effectively by choosing the focal mode of the applicator as it is predicted by theoretical analysis.

Key words: Ultrasound, phased array, diffused foci, tissue phantom

1. Introduction

Ultrasound has tissue absorption and attenuation coefficients appropriate for non-invasive non-superficial hyperthermia at wavelengths much smaller than the size of the human body. This is a unique advantage when compared to electromagnetic modalities, and allows ultrasound to penetrate deep inside the body while maintaining the ability to focus energy into small volumes in non-superficial tissues.

In order to generate precise time-averaged power deposition patterns to heat tumours, a sharp ultrasound focal spot can be mechanically scanned (Lele 1983) or electronically scanned (Ocheltree *et al.* 1984, Ebbini *et al.* 1988). Another approach is to produce diffuse focal patterns directly, without scanning, using multiple transducers (Fessenden *et al.* 1984), or using phased arrays (Do Huu and Hartmann 1982, Cain and Umemura 1986, Umemura *et al.* 1986, Ibbini and Cain 1989).

The 'sector-vortex' phased array was proposed for precise direct synthesis of small annular heating patterns, and a prototype applicator has been constructed (Umemura and Cain 1987). Unwanted secondary foci, which tend to be produced beyond or in front of diffuse focal fields, are eliminated by the phase modulation along the focal annuli (Umemura and Cain 1989). Large intensity gain can be obtained from a reasonably small number of elements, since the applicator uses two-dimensional geometric focusing. It can also be used for electronic scanning of a focal spot in a region around the geometric focus (Umemura and Cain 1988).

In the evaluation of heating efficacy of a prototype applicator for hyperthermia, perfusion is an essential factor to be simulated, as well as the energy absorption properties (Lele and Parker 1982, Roemer *et al.* 1984, Umemura *et al.* 1988, Hynynen *et al.* 1989, Prionas *et al.* 1991). A perfused tissue phantom was used in this study, which consisted of a fixed

porcine kidney perfused with degassed water by a variable flow rate pump (Holmes *et al.* 1983, Benkeser *et al.* 1990).

In what follows, the prototype sector-vortex applicator is first described, followed by the description of the perfused phantom. The elevated temperature patterns in the phantom resulting from the insonation experiments with the annular focal fields produced by the applicator are then compared to the theoretical analysis and discussed.

2. Methods and materials

2.1. *A prototype sector-vortex array applicator*

The configuration of the prototype sector-vortex phased array applicator used in the insonation experiments is shown in Figure 1 (Umemura and Cain 1992). It has 32 transducer elements (16 sectors×2 tracks) mounted on polished flats machined on the outer surface of a spherical shell having a radius of curvature of 120 mm for geometric focusing. Outer radii of outside and inside tracks of the array transducer are r_2=60 mm and r_1=40 mm, respectively. A central hole in the transducer with radius r_0=20 mm is reserved for an ultrasound imaging probe.

A modified lead–titanate ceramic (Takeuchi *et al.* 1982) was employed for the transducer elements in order to minimize the potential problem of unwanted lateral mode resonances in individual elements. Aluminium was chosen for the shell material so that the shell provides good acoustic impedance matching and efficient cooling. It also forms the ground electrode for all elements. A low thermal expansion epoxy adhesive (Eccobond 285,

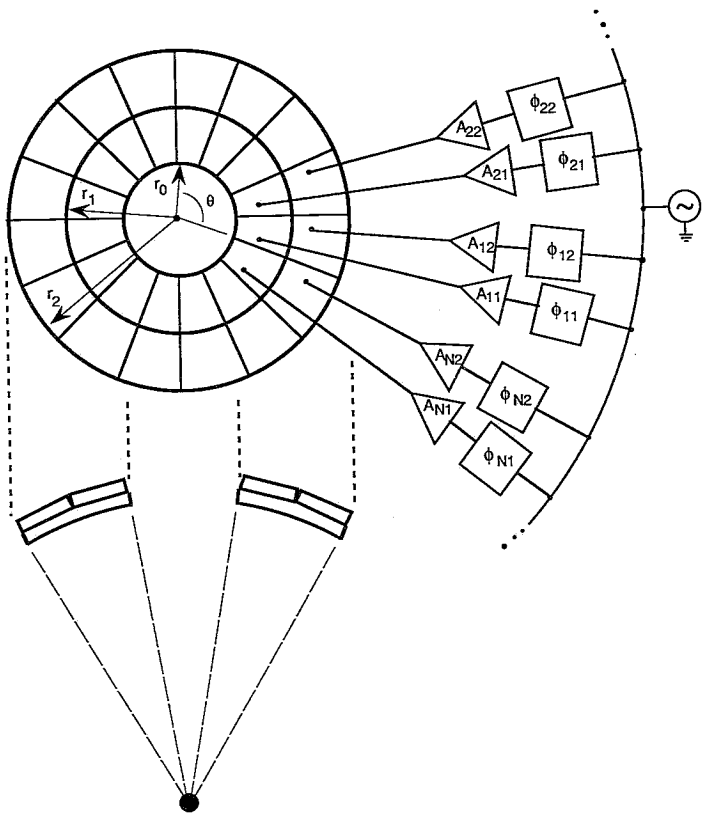

Figure 1. Schematic of sector-vortex array configuration; ϕ_{11}, ϕ_{12}, ϕ_{21}, ϕ_{22},... denote phase shifters, while A_{11}, A_{12}, A_{21}, A_{22},... denote amplifiers.

Emerson and Cuming) was used to attach the ceramic elements to the aluminium shell tightly. The elements were driven at an ultrasound frequency of 750 kHz in the insonation experiments. The thickness of the aluminium shell was chosen to be a quarter-wavelength at 750 kHz at the centre of each element.

Each of the 32 elements is driven by an individual amplifier consisting of a complementary pair of high-speed power MOS FETs. The phase of the digitally generated square-wave driving signal is discretized into a multiple of $2\pi/16$ as specified by a four-bit binary code from a control computer (PC 6300, AT&T) using DMA transfer, enabling fast temporal switching between different focusing modes within 1 ms if necessary. An inductance and capacitance are electrically connected in series and parallel with each transducer element, respectively, for reducing the harmonic components in the driving waveform. The third harmonic (2250 kHz) amplitude was less than 1% of the primary component (750 kHz).

In order to produce annular focal fields, the nth elements on the inside and outside tracks are driven by the signals whose complex amplitudes are represented by A_{n1} and A_{n2} in equations (1) and (2) respectively:

$$A_{n1}=A_0 \exp[j(M\theta_n-\omega t)] \tag{1}$$

$$A_{n2}=A_{n1} \exp(j\gamma). \tag{2}$$

Here, M is the mode number such that $-8\leq M\leq 8$; θ_n is the angular coordinate of the nth element position given by $\theta_n=2\pi\, n/16$ ($n=1, 2, \ldots, 16$), ω is the ultrasound angular frequency, and γ is the drive phase difference between the two tracks. Both equations give phase distributions which rotate $|M|$ times around the disc clockwise ($M<0$) or counter-clockwise ($M>0$).

An annular focal field approximated by the $|M|$th-order Bessel function is predicted to be formed by each track. When $\gamma=0$ the applicator is equivalent to a single-track 16-element sector-vortex array with outer and inner radii of r_2 and r_0, respectively. When $\gamma\sim\pi$ the interference between the two annular fields was predicted to produce some useful enhancements of the intensity patterns (Umemura and Cain 1989). These predictions have been verified by three-dimensional acoustic field measurement using a 21-channel membrane probe (Y–33–6525, GEC-Marconi) consisting of a co-planer spot-poled 25 μm PVDF (polyvinylidene fluoride) film membrane. The measured patterns compared very well with the fields theoretically predicted by computer simulation (Umemura and Cain 1987). The absolute acoustic power on the focal plane was calibrated against the applied electric power to the power MOS FETs by measuring radiation force on a rectangular hollow brass plate (Benkerser *et al.* 1987). Details of the acoustical evaluation of the applicator are described in the previous paper (Umemura and Cain 1992).

2.2. *Perfused tissue phantom*

The perfused tissue phantom consisting of an alcohol-fixed porcine kidney was insonated by the prototype applicator. It was fixed by perfusion with a graded series of ethyl alcohol mixtures immediately after excision (Holmes *et al.* 1984). The tissue was stored in alcohol and rehydrated with degassed water for several hours prior to the insonation, to remove all traces of alcohol from the tissue. The specific heat was estimated from the H_2O content to be approximately $3{\cdot}8\ \mathrm{Jg^{-1}{}^{\circ}C^{-1}}$ (Benkeser *et al.* 1990).

The phantom was mounted in a PMMA (poly methyl methacrylate) frame using two 20-gauge injection needles at its lateral ends as shown in Figure 2. Sixteen 0·1 mm wire size chromel–constantan thermocouples were carefully placed in the cortex with 2·54 mm

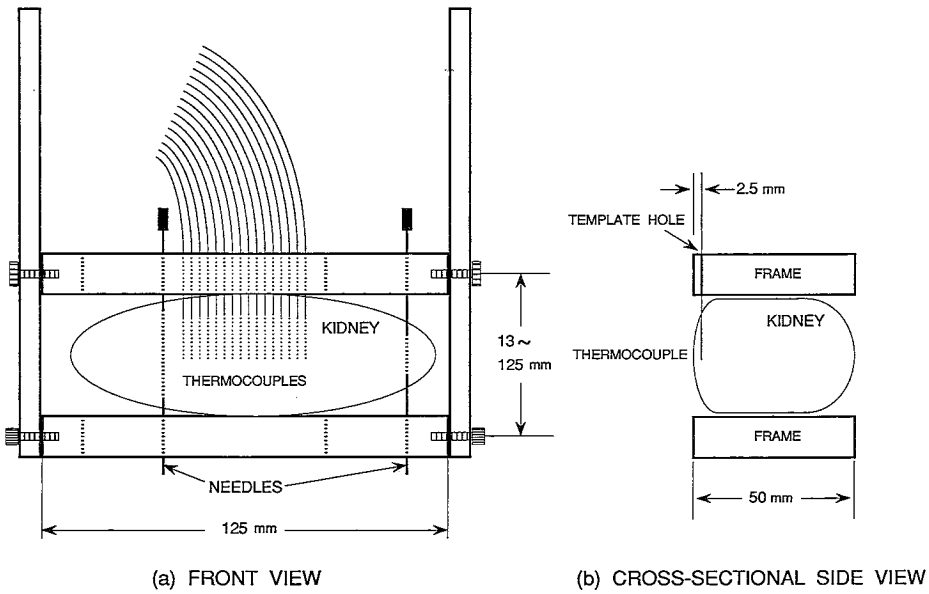

Figure 2. Configuration of mounting fixed porcine kidney in PMMA frame: (**a**) front view; (**b**) cross-sectional side view.

spacing at 2·5 mm from the surface of the kidney using 25-gauge injection needles through template holes in the frame. A small thermocouple wire size was chosen to make temperature artifacts due to viscous heating (Goss *et al.* 1977) and due to thermal conductance through the wires as small as possible, while maintaining the appropriate rigidity for handling. Each thermocouple was made by soldering two wires using as small an amount of solder as possible. After the thermocouples were inserted with the needles into the cortex, the needles were removed from the cortex leaving the thermocouple wires in place. The distance of each thermocouple from the surface was checked by imaging the wire position with a 10 MHz ultrasound ophthalmic diagnosis system (Ocuson 400, Sonometrics Systems, Inc.).

The instrumented kidney and frame were then placed in a temperature-controlled water tank filled with 175 l of degassed water at 37°C, which served as the coupling medium as well as the perfusate. A calibrated, variable flow rate roller pump was connected to the renal artery of the kidney and circulated the degassed water. The renal vein was allowed to drain directly into the tank. The pump produced flow rates similar to those found in human tissues. Perfusion was calculated from total flow rates divided by the volume of the kidney, which was estimated from its weight after rehydration. The kidney was located so that the thermocouples in the cortex were aligned in the geometric focal plane of the array transducer. A side view of the experimental set-up in the tank is shown in Figure 3.

The thermocouples were connected to a 16-channel thermometry board (Exp-16, MetraByte) installed in the same computer that controlled the array transducer. Instead of using the cold junction compensation circuitry on the board, the reference cold junction for each thermocouple was placed in the degassed water in the tank for better accuracy and stability. The temperature data with an accuracy of 0·1°C were acquired from all channels once a second. The temperature drift in 2 h was not more than 0·3°C. Temperature distributions were measured only after a thermal steady state was reached following the initiation of insonation, and immediately after the insonation was temporarily stopped.

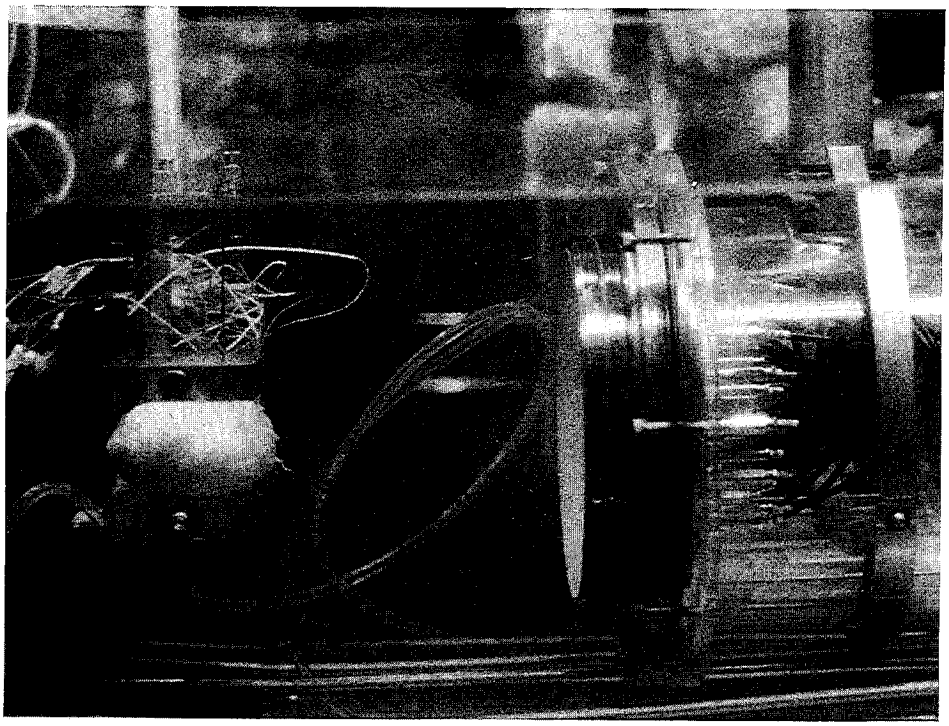

Figure 3. Side view of experimental set-up for insonation of perfused fixed porcine kidney.

It took about 5 min when the kidney was not perfused, but much shorter when it was perfused.

The temperature drop directly after the stop of insonation, which is known to correspond to the temperature artifact due to viscous heating in the vicinity of the wires, was not more than the temperature drift described above. All the temperature patterns presented were obtained using the same single fixed kidney. The reproducibility of the temperature pattern was verified by insonations with the same mode number at the same drive voltage both at the beginning and at the end of the series of experiments.

2.3. *Theoretical analysis*

In order to predict and interpret the change in the measured temperature distribution patterns due to the focal mode number and the perfusion rate, the temperature distribution was theoretically analysed. The steady-state version of the bioheat equation (Pennes 1948) was numerically solved using a finite difference technique with the method of successive displacements with over-relaxation (Forsythe and Wasow 1960).

A simple thermal model, shown in Figure 4, was employed for the theoretical analysis in order to minimize the number of adjustable parameters difficult to measure. Cylindrical symmetry was assumed in the model because the surface of the kidney was reasonably flat in the region of the focal annuli. The radius of the surface curvature in the region was much larger than both the distance from the surface to the points where the temperature was measured (2·5 mm) and the radius of the largest focal annulus (10 mm). The depth of the model (100 mm) was chosen much larger than the actual thickness of the kidney, since the heat transfer through the front surface (facing the applicator) of the kidney was the main concern rather than the heat transfer through the rear surface. The size of the

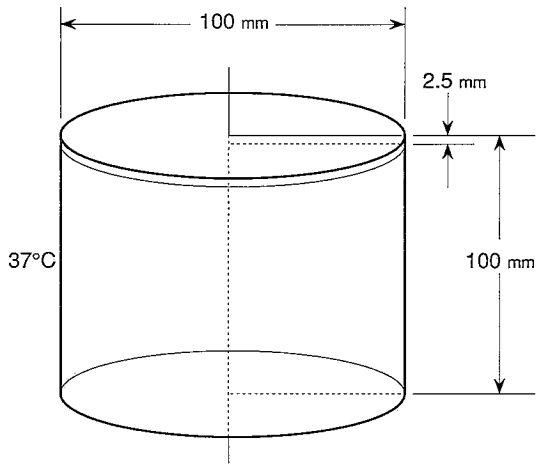

Figure 4. Simplified cylindrical thermal model for theoretical computation. The focal plane and the temperature measurement points were located 2·5 mm from the surface for the computation for Figure 5. A surface temperature of 37°C served as a boundary condition. Perfusion rate, thermal conductivity, and specific heat were assumed to be uniform throughout the model.

cylindrical model was 100 mm both in diameter and depth. Two-dimensional steady-state temperature distributions were calculated by discretizing the 50×100 mm rectangular cross-section into 0·25×0·25 mm squares.

A surface boundary temperature was assumed to be 37°C at all surfaces of the cylindrical model, ignoring the temperature gradient in the boundary layer of coupling water in the vicinity of the front surface of the kidney. Perfusion rates, thermal conductivity (0·55 $Wm^{-1}°C^{-1}$), and specific heat (3·8 $Jg^{-1}°C^{-1}$) were assumed to be uniform throughout the model.

The ultrasound power deposition pattern needed for the temperature analysis was computed for each focal mode number by quantizing the transducer into numerous point sound sources separated by less than a half wavelength and summing up all of their contributions to the acoustic field. The ultrasound attenuation coefficient in the computation was assumed to be 0·044 nepers $cm^{-1}Hz^{-1}$ (0·38 dB $cm^{-1}Hz^{-1}$) throughout the cylindrical model, which was obtained from the measured absorption coefficient of the rehydrated kidney fixed in the same procedure (Benkeser *et al.* 1990) assuming the attenuation due to scattering is negligible compared to the attenuation due to absorption. Scattering which may occur at the front surface of the kidney, and possible effects of nonlinear propagation, are ignored. The array transducer was assumed to have an infinite number of sectors in the computation in order to force the power deposition patterns to have cylindrical symmetry.

All computations used a Hitac S-810 supercomputer (Hitachi Ltd). Typical computation times to obtain ultrasound power deposition and temperature distribution patterns were 350 and 90 s, respectively.

3. Results and discussion

The measured and theoretical steady-state temperature distribution patterns along a diameter in the focal plane in the cortex are shown in Figure 5 for the mode number $M=0$, 2, 4, 6, and 8, with no phase difference between the tracks ($\gamma=0$). The patterns with the phase difference, $\gamma=\pi$, are plotted in Figure 6 for the mode number $M=8$. The kidney

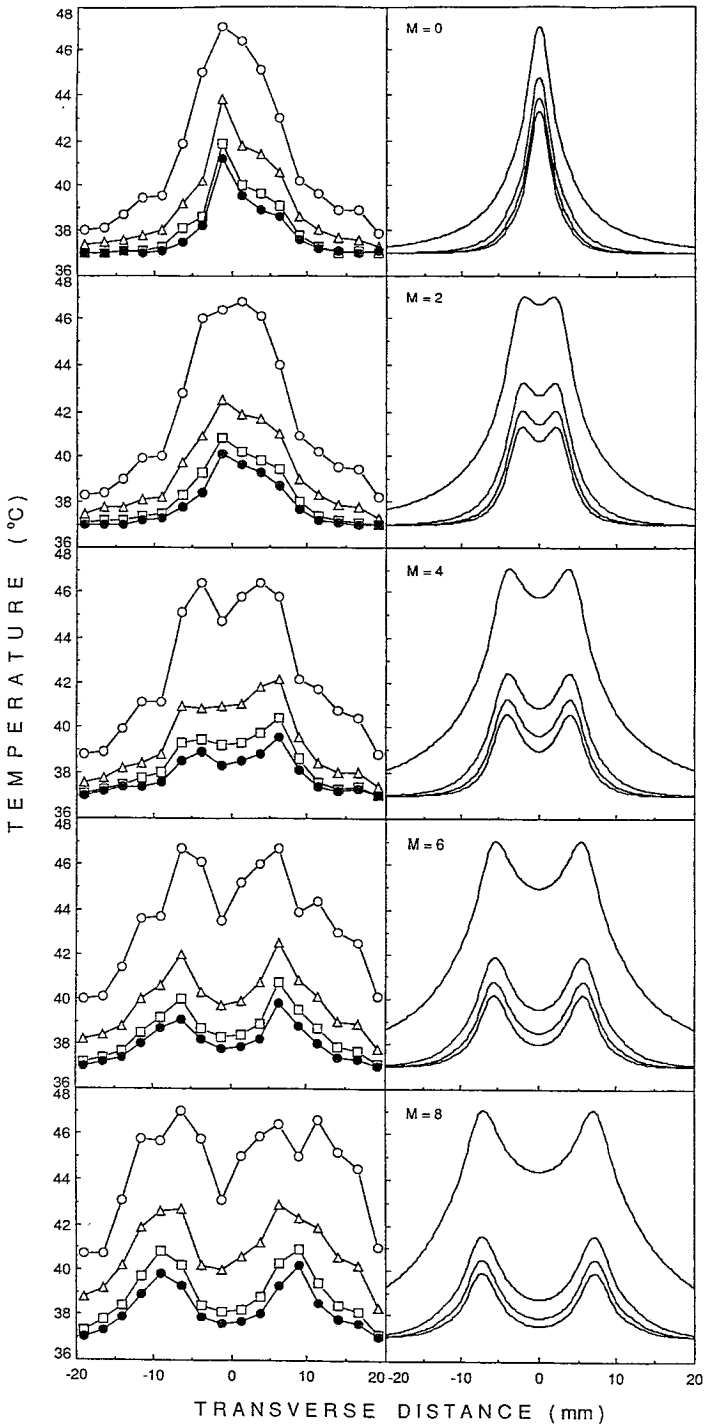

Figure 5. Temperature distributions in cortex of fixed porcine kidney insonated with mode number M=0, 2, 4, 6, 8 and γ=0; plotted curves are 0 (○), 7 kg m^{-3} s^{-1} (△), 15 kg m^{-3} s^{-1} (□), 23 kg m^{-3} s^{-1} (●).

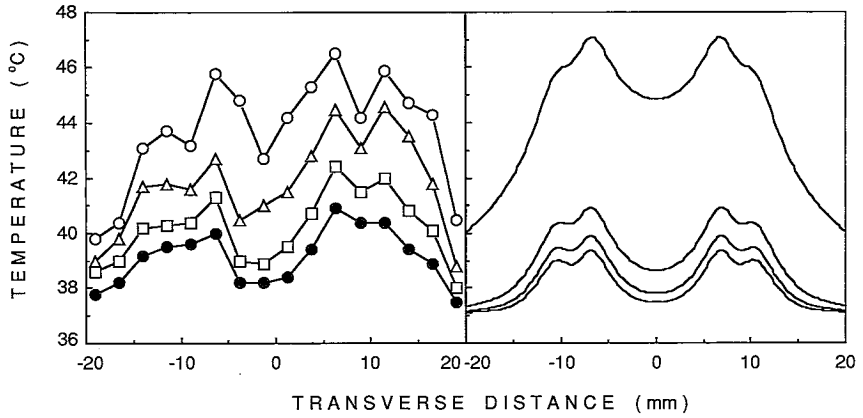

Figure 6. Temperature distributions from mode number $M=8$ and $\gamma=\pi$; left: measurement; right: theory. Perfusion rates for the four plotted curves are the same as in Figure 5.

Table 1. Focal acoustic power (W).

	$M=0$	$M=2$	$M=4$	$M=6$	$M=8$	
			$\gamma=0$			$\gamma=\pi$
Measurement	12	15	18	26	38	48
Theory	4·2	7·7	11·5	15·5	20·0	25·0

Table 2. Average radius of heated region (mm).

Perfusion (kg m^{-3} s^{-1})	$M=0$	$M=2$	$M=4$	$M=6$	$M=8$	
			$\gamma=0$			$\gamma=\pi$
0	6·1	6·5	7·4	8·5	9·2	9·2
7	5·3	5·9	6·6	8·3	9·1	9·4
15	3·8	4·6	6·0	7·7	8·7	9·6
23	3·6	3·9	5·9	7·3	8·5	9·5

was perfused at the rates of 0, 7, 15, 23 kg m^{-3} s^{-1} in each figure. The drive voltage of the array transducer was adjusted so that the spatial peak temperature reaches about 47°C with no perfusion, and it was kept the same throughout all experiments for each mode number. The magnitude of the ultrasound power deposition in the theoretical analysis was also adjusted in the same way. The focal acoustic power estimated from the applied electric power to the transducer in the measurement and the focal acoustic power assumed in the theoretical analysis are listed in Table 1.

Although the measured temperature distribution patterns are relatively broader and irregular in comparison with the corresponding theoretical pattern, the measurement and theory agree well in the overall dependence of the heated region widths on the mode number M as seen in Figure 5. They also agree in the overall dependence on perfusion rate.

The average radius of the heated region, R, defined by

$$R=\sum|r_k|\,T_k/\sum T_k \tag{3}$$

where r_k and T_k are the transverse distance from the axis and the temperature rise of the kth measurement point, respectively, was calculated from the measured temperature distribution in each figure and is listed in Table 2. In Figure 7 the radius R is plotted as

a function of the mode number M (for $\gamma=0$) for perfusion rates of 0 and 23 kg m^{-3} s^{-1}. The values from the theoretical computations are also plotted for comparison. The average radius of the heated region can be increased by a factor of approximately 2 (from 3–6 mm up to 8–9 mm) by increasing the mode number M from 0 to 8. In addition, the heated region width becomes less sensitive to the perfusion rate as the mode number M increases, as predicted by the theory.

It is apparent for each mode number in Figure 5 that the discrepancy between the measurement and the theory is relatively large at low perfusion rates such as 7 kg m^{-3} s^{-1}. Choosing $M=6$ as an example, the average temperature rise normalized to the temperature rise without perfusion was plotted in Figure 8 for both the measurement and the theory as a function of perfusion rate.

In deep tissues it was theoretically predicted that the central region can be heated equally to the periphery with a single annular pattern when it is poorly perfused (Umemura and Cain 1990). However, in Figure 5 a dip was seen at the centre of each measured and theoretical pattern for $M=4$, 6, and 8. In comparison, temperature distributions for $M=6$ were computed for the situation where the focal plane is located in the model 15 mm from

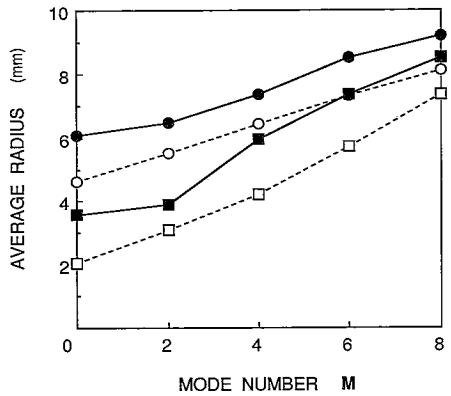

Figure 7. Average radius of heated region plotted against mode number M for $\gamma=0$; circles for no perfusion; squares for perfusion rate of 23 kg m^{-3} s^{-1}; solid circles and squares for measurement; and open circles and squares for theory.

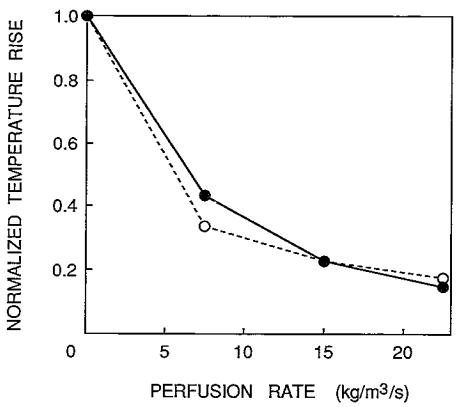

Figure 8. Normalized average temperature rise as function of perfusion rate for $M=6$; solid circles for measurement; and open circles for theory.

the surface. The temperature distribution patterns on the focal plane are plotted in Figure 9. The focal acoustic power was assumed to be the same as for $M=6$ in Figure 5. Only a slight dip is seen in the temperature distribuition without perfusion (the top curve) and the temperature rise is about three times as much as the corresponding distribution in Figure 5, whereas the temperature distributions with perfusion are similar. Note that in Figure 9 the temperature axis scale is half that in Figure 5.

These results suggest that substantial heat was lost through the front surface of the kidney in the experiment. Because of this heat transfer process, central temperature dips were produced even for no perfusion, and higher ultrasound power was required to raise the temperature. This could be one limitation of the use of the perfused kidney phantom as a model of perfused deep tissues. Since the heat loss through the surface boundary is significant, the employed boundary condition ignoring the temperature gradient in the coupling water boundary layer might introduce error. However, this simplified boundary condition may not be the most important cause for the discrepancy between the measurement and the theory, since the difference between the theoretical temperature distributions with and without perfusion would become even larger, and the discrepancy seen in Figure 8 would become more significant, if the temperature gradient in the coupling water boundary layer is taken into account.

The possible heat loss through the thermocouple wires, which was ignored in the theoretical analysis, might have decreased the difference between the measured temperature distributions with and without perfusion, and caused the discrepancy seen in Figure 8. Although the perfusion in the cortex is relatively uniform compared to the other parts of the kidney, the irregularity seen in the measured patterns might have been caused by the non-uniformity or the directivity of the perfusion in the cortex, since it was reproducible for the particular kidney. Further investigation into the distribution and directivity of the microvascular system in the cortex and application of a more sophisticated formulation (Weinbaum and Jiji 1985) rather than the classical bioheat equation might decrease the discrepancy between measurement and theory.

Attenuation, diffraction, and nonlinear propagation of ultrasound taking place in the tissues intervening between the skin surface and the deep tissue, where the foci may be

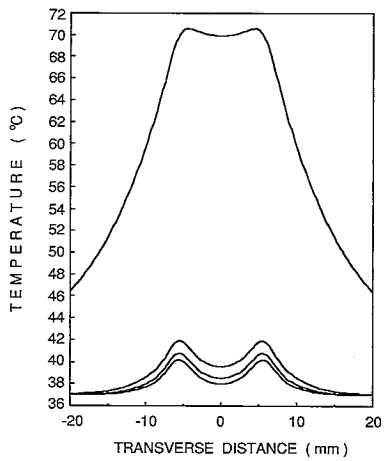

Figure 9. Temperature distributions from theoretical computation for mode number $M=6$ and $\gamma=0$ in focal plane located 15 mm from surface. Perfusion rates for the four plotted curves are the same as in Figure 5.

located, were not considered in the experimental set-up. These should also be taken into account in real clinical situations.

4. Conclusion

The control of heating patterns by changing the mode number of the sector-vortex array applicator was demonstrated in insonation experiments with a perfused porcine kidney phantom. The average radius of the heated region can be changed from about 5 mm up to 9 mm by increasing the mode number M from 0 to 8. It was tested with the perfusion rates ranging from 0 up to 23 kg m^{-3} s^{-1}, which covers most situations in human tissues. The results suggest that the prototype array applicator should be able to heat superficial or deep tumours with diameters ranging from about 10 mm up to about 20 mm.

Acknowledgements

The authors thank S. Saito, of the Central Research Laboratory, Hitachi Ltd, Tokyo, Japan (HCRL), for his careful redesign for precision machining of the transducer shell and housing, and B. B. McNeill and J. W. Cobb, with the Bioacoustics Research Laboratory, University of Illinois (BRL), for their helpful cooperation in the design and construction of apparatus for measurements; F. Haymann, a student at BRL, for his cooperation in writing the program to control the array transducer; R. Camello and S. Chen, also students at BRL, for their cooperation in writing the program to control the temperature measurement system; M. Ibbini and E. Ebbini, with BRL, for useful discussions, and K. Katakura with HCRL for his support. This work was funded in part by NIH Grant CA 44124 and an award from HCRL.

References

BENKESER, P. J., FRIZZELL, L. A., OCHELTREE, K. B. and CAIN, C. A., 1987, A tapered phased array ultrasound transducer for hyperthermia treatment. *IEEE Transactions in Ultrasonics, Ferroelectrics, and Frequency Control,* **UFFC-34**(4), 446–453.

BENKESER, P. J., FRIZZELL, L. A., HOLMES, K. R. and GOSS, S. A., 1990, A perfused tissue phantom for ultrasound hyperthermia. *IEEE Transactions in Biomedical Engineering,* **BME-37**(2), 425–428.

CAIN, C. A. and UMEMURA, S., 1986, Concentric-ring and sector-vortex phased array for tumor treatment. *IEEE Transactions in Microwave Theory and Technology,* **MTT-34,** 542–551.

DOHUU, J. and HARTMANN, P., 1982, Deep and local heating by an ultrasound phased array transducer. *Proceedings of 1982 IEEE Ultrasonics Symposium,* pp. 735–738.

EBBINI, E. S., UMEMURA, S., IBBINI, M. S. and CAIN, C. A., 1988, A cylindrical-section ultrasound phased array applicator for cancer therapy. *IEEE Transactions in Ultrasonics Ferroelectrics and Frequency Control,* **UFFC-35**(5), 651–572.

FESSENDEN, P., LEE, E. R., ANDERSON, T. L., STROHBEHN, J. W., MEYER, J. L., SAMULSKI, T. V. and MARMOR, J. B., 1984, Experience with a multitransducer ultrasound system for localized hyperthermia of deep tissues. *IEEE Transactions in Biomedical Engineering,* **BME-31,** 126–135.

FORSYTHE, G. E. and WASOW, W. R., 1960, *Finite Difference Methods for Partial Differential Equations* (New York: Wiley).

GOSS, S. A., COBB, J. W. and FRIZZELL, L. A., 1977, Effect of beam width and thermocouple size on the measurement of ultrasonic absorption using the thermoelectric technique. *Proceedings of 1977 IEEE Ultrasonics Symposium,* pp. 206–211.

HOLMES, K. R., RYAN, W., WEINSTEIN, P. and CHEN, M. M., 1984, A fixation technique for organs to be used as perfused tissue phantoms in bioheat transfer studies. *1984 Advances in Bioengineering*, edited by R. L. Spiker (New York: American Society of Mechanical Engineers), pp. 9–10.

HYNYNEN, K., DEYOUNG, D., KUNDRAT, M. and MOROS, E., 1989, The effect of blood perfusion rate on the temperature distributions induced by multiple, scanned and focused ultrasonic beams in dogs' kidney *in vivo. International Journal of Hyperthermia,* **5**(4), 485–497.

IBBINI, M. S. and CAIN, C. A., 1989, A field conjugation method for direct synthesis of hyperthermia phased-array heating patterns. *IEEE Transactions in Ultrasonics, Ferroelectrics and Frequency Control,* **UFFC-36**(1), 3–9.

LELE, P. P., 1983, Physical aspects and clinical study with ultrasound hyperthermia. *Hyperthermia in Cancer,* edited by F. C. Storm (Boston: Hall Medical Publishers), pp. 333–367.

LELE, P. P. and PARKER, K. J., 1982, Temperature distribution in tissues during local hyperthermia by stationary or steered beams of unfocused or focused ultrasound. *British Journal of Cancer,* **45** (Suppl. V), 108–121.

OCHELTREE, K. B., BENEKESER, P. J., FRIZZELL, L. A. and CAIN, C. A., 1984, An ultrasonic phased-array applicator for hyperthermia. *IEEE Transactions in Sonics and Ultrasonics,* **SU-31,** 526–531.

PENNES, H. H., 1948, Analysis of tissue and arterial blood temperature in resting forearm. *Journal of Applied Physiology,* **1,** 93–122.

PRIONAS, S. D., RAFTERY, K. A., EDMONDS, P. D. and CONSTANTINOU, C. E., 1981, Flow-dependence of 2-D temperature distributions induced perfused canine kidney by ultrasound. *International Journal of Hyperthermia,* 7(2), 363–383.

ROEMER, R. B., SWINDELL, W., CLEGG, S. T. and KRESS, R. L., 1984, Simulation of focused, scanned ultrasonic heating of deep seated tumors: the effect of blood perfusion. *IEEE Transactions in Sonics and Ultrasonics,* **SU-31,** 457–466.

TAKEUCHI, H., JYOMURA, S., YAMAMOTO, E. and ITO, Y., 1982, Electromechanical properties of $(Pb,Ln)(Ti,Mn)O_3$ ceramics (Ln=rare earths). *Journal of the Acoustical Society of America,* **72**(4), 1114–1120.

UMEMURA, S. and CAIN, C. A., 1987, Evaluation of a prototype sector-vortex array applicator. *Proceedings of 1987 IEEE Ultrasonics Symposium,* pp. 867–870.

UMEMURA, S. and CAIN, C. A., 1988, Theoretical study of acoustic and thermal fields generated by phased array systems. *Proceedings of 5th International Symposium on Hyperthermic Oncology,* **2,** 674–677.

UMEMURA, S. and CAIN, C. A., 1989, The sector-vortex phased array: acoustic field synthesis for hyperthermia. *IEEE Transactions in Ultrasonics, Ferroelectrics and Frequency Control,* **UFFC-36**(2), 249–257.

UMEMURA, S. and CAIN, C. A., 1990, Analysis of temperature responses to diffused ultrasound focal fields produced by a sector-vortex phased array. *International Journal of Hyperthermia,* **6**(3), 641–654.

UMEMURA, S. and CAIN, C. A., 1992, Acoustical evaluation of a prototype sector-vortex phased array applicator. *IEEE Transactions in Ultrasonics Ferroelectrics and Frequency Control,* **UFFC-39**(1), 32–38.

UMEMURA, S., CAIN, C. A. and KATAKURA, K., 1986, Acoustic field synthesis by sector-vortex array for tumor treatment. *Proceedings of 1986 IEEE Ultrasonics Symposium,* pp. 967–971.

UMEMURA, S., CAIN, C. A. and HOLMES, K. R., 1988, Evaluation of a prototype sector-vortex phased. array applicator. *Proceedings of 5th International Symposium on Hyperthermic Oncology,* **1,** 906–907.

WEINBAUM, S. and JIJI, L. M., 1985, A new simplified bioheat equation for the effect of blood flow on local average tissue temperature. *Journal of Biomechanical Engineering,* **107,** 131–139.

52